Alexandria Engineering Journal (2015) 54, 829–841

HOSTED BY

ELSEVIER

Alexandria University

Alexandria Engineering Journal

www.elsevier.com/locate/aej
www.sciencedirect.com

REVIEW

Numerical study of flow and heat transfer of non-Newtonian Tangent Hyperbolic fluid from a sphere with Biot number effects

S. Abdul Gaffar [a], V. Ramachandra Prasad [b,*], O. Anwar Bég [c]

[a] *Department of Mathematics, Salalah College of Technology, Salalah, Oman*
[b] *Department of Mathematics, Madanapalle Institute of Technology and Science, Madanapalle 517325, India*
[c] *Gort Engovation Research (Aerospace), 15 Southmere Avenue, Great Horton, Bradford BD7 3NU, West Yorkshire, UK*

Received 1 September 2014; revised 23 March 2015; accepted 4 July 2015
Available online 20 July 2015

KEYWORDS

Non-Newtonian Tangent Hyperbolic fluid;
Skin friction;
Weissenberg number;
Power law index;
Boundary layer flow;
Biot number

Abstract In this article, we investigate the nonlinear steady boundary layer flow and heat transfer of an incompressible Tangent Hyperbolic fluid from a sphere. The transformed conservation equations are solved numerically subject to physically appropriate boundary conditions using implicit finite-difference Keller Box technique. The numerical code is validated with previous studies. The influence of a number of emerging non-dimensional parameters, namely Weissenberg number (*We*), power law index (*n*), Prandtl number (*Pr*), Biot number (γ) and dimensionless tangential coordinate (ξ) on velocity and temperature evolution in the boundary layer regime is examined in detail. Furthermore, the effects of these parameters on heat transfer rate and skin friction are also investigated. Validation with earlier Newtonian studies is presented and excellent correlation is achieved. It is found that the velocity, Skin friction and the Nusselt number (heat transfer rate) are decreased with increasing Weissenberg number (*We*), whereas the temperature is increased. Increasing power law index (*n*) increases the velocity and the Nusselt number (heat transfer rate) but decreases the temperature and the Skin friction. An increase in the Biot number (γ) is observed to increase velocity, temperature, local skin friction and Nusselt number. The study is relevant to chemical materials processing applications.

* Corresponding author.
E-mail address: rcpmaths@gmail.com (V.R. Prasad).
Peer review under responsibility of Faculty of Engineering, Alexandria University.

http://dx.doi.org/10.1016/j.aej.2015.07.001

Nomenclature

a	radius of the sphere
C_f	skin friction coefficient
f	non-dimensional steam function
Gr	Grashof number
g	acceleration due to gravity
k	thermal conductivity of fluid
n	power law index
Nu	local Nusselt number
Pr	Prandtl number
$r(x)$	radial distance from symmetrical axis to surface of the sphere
T	temperature of the fluid
u, v	non-dimensional velocity components along the x- and y-directions, respectively
V	velocity vector
We	Weissenberg number
x	stream wise coordinate
y	transverse coordinate

Greek

α	thermal diffusivity
η	the dimensionless radial coordinate
μ	dynamic viscosity
ν	kinematic viscosity
θ	non-dimensional temperature
ρ	density of non-Newtonian fluid
ξ	the dimensionless tangential coordinate
ψ	dimensionless stream function
γ	Biot number
Γ	time dependent material constant
Π	second invariant strain tensor

Subscripts

w	conditions at the wall (sphere surface)
∞	free stream conditions

Contents

1. Introduction

The dynamics of non-Newtonian fluids has been a popular area of research owing to ever-increasing applications in chemical and process engineering. Examples of such fluids include coal-oil slurries, shampoo, paints, clay coating and suspensions, grease, cosmetic products, custard, and physiological liquids (blood, bile, synovial fluid). The classical equations employed in simulating Newtonian viscous flows i.e. the Navier–Stokes equations fail to simulate a number of critical characteristics of non-Newtonian fluids. Hence several constitutive equations of non-Newtonian fluids have been presented over the past decades. The relationship between the shear stress and rate of strain in such fluids is very complicated in comparison with viscous fluids. The viscoelastic features in non-Newtonian fluids add more complexities in the resulting equations when compared with Navier–Stokes equations. Significant attention has been directed at mathematical and numerical simulation of non-Newtonian fluids. Recent investigations have implemented, respectively the Casson model [1], second-order Reiner–Rivlin differential fluid models [2], power-law nanoscale models [3], Eringen micro-morphic models [4] and Jeffreys viscoelastic model [5].

Convective heat transfer has also mobilized substantial interest owing to its importance in industrial and environmental technologies including energy storage, gas turbines, nuclear plants, rocket propulsion, geothermal reservoirs, and photovoltaic panels. The convective boundary condition has also attracted some interest and this usually is simulated via a Biot number in the wall thermal boundary condition. Recently, Ishak [6] discussed the similarity solutions for flow and heat transfer over a permeable surface with convective boundary condition. Aziz [7] provided a similarity solution for laminar thermal boundary layer over a flat surface with a convective surface boundary condition. Aziz [8] further studied hydrodynamic and thermal slip flow boundary layers with an iso-flux thermal boundary condition. The buoyancy effects on thermal boundary layer over a vertical plate subject with a convective surface boundary condition were studied by Makinde and Olanrewaju [9]. Further recent analyses include Makinde and Aziz [10]. Gupta et al. [11] used a variational finite element to simulate mixed convective–radiative micropolar shrinking sheet flow with a convective boundary condition. Makinde et al. [12] studied cross diffusion effects and Biot number influence on hydromagnetic Newtonian boundary layer flow with homogenous chemical reactions and **MAPLE** quadrature routines. Bég et al. [13] analyzed Biot number and buoyancy effects on magnetohydrodynamic thermal slip flows. Subhashini et al. [14] studied wall transpiration and cross

diffusion effects on free convection boundary layers with a convective boundary condition.

An interesting non-Newtonian model developed for chemical engineering systems is the Tangent Hyperbolic fluid model. This rheological model has certain advantages over the other non-Newtonian formulations, including simplicity, ease of computation and physical robustness. Furthermore it is deduced from kinetic theory of liquids rather than the empirical relation. Several communications utilizing the Tangent Hyperbolic fluid model have been presented in the scientific literature. There is no single non-Newtonian model that exhibits all the properties of non-Newtonian fluids. Among several non-Newtonian fluids, hyperbolic tangent model is one of the non-Newtonian models presented by Pop and Ingham [15]. Nadeem and Akram [16] made a detailed study on the peristaltic transport of a hyperbolic tangent fluid in an asymmetric channel. Nadeem and Akram [17] investigated the peristaltic flow of a MHD hyperbolic tangent fluid in a vertical asymmetric channel with heat transfer. Akram and Nadeem [18] analyzed the influence of heat and mass transfer on the peristaltic flow of a hyperbolic tangent fluid in an asymmetric channel. Akbar et al. [19] analyzed the numerical solutions of MHD boundary layer flow of tangent hyperbolic fluid on a stretching sheet. Akbar et al. [20] studied the peristaltic flow of tangent hyperbolic fluid with convective boundary condition. Peristaltic flow of hyperbolic tangent fluid in a diverging tube with heat and mass transfer is studied by Nadeem et al. [21]. Akbar et al. [22] investigated the peristaltic flow of a tangent hyperbolic fluid in an inclined asymmetric channel with slip and heat transfer. Akbar et al. [23] also made a detailed study on the effects of heat and mass transfer on the peristaltic flow of hyperbolic tangent fluid in an annulus.

In many chemical engineering and nuclear process systems, *curvature of the vessels employed* is a critical aspect of optimizing thermal performance. Examples of curved bodies featuring in process systems include torus geometries, wavy surfaces, cylinders, cones, ellipses, oblate spheroids and in particular, spherical geometries, the latter being very popular for storage of chemicals and also batch reactor processing. Heat transfer from spheres has therefore mobilized much attention among chemical engineering researchers who have conducted both experimental and computational investigations for both Newtonian and non-Newtonian fluids. Amato and Chi [24] studied experimentally natural convection from heated spheres in water for an extensive range of Rayleigh numbers and for laminar, transitional and early turbulent flow using hot-film anemometry techniques. Liew and Adelman [25] conducted experiments on free convection heat transfer from an isothermal sphere to water and various aqueous polymer solutions (power-law fluids), elucidating the influence of flow behavior index and consistency index. Further empirical investigations were reported by Amato and Chi [26] for aqueous polymer solutions using hot-film anemometry and Churchill [27], the latter deriving expressions for local and mean Nusselt number for natural convection from an isothermal sphere as a function of the Rayleigh and Prandtl numbers valid for laminar boundary layers. Lien and Chen [28] used a finite difference code to simulate laminar mixed (forced and free) convection flow of an Eringen micropolar fluid from a permeable sphere with surface suction/injection effects. Jia and Gogos [29] analyzed computationally the steady free convection from a sphere for an extensive range of Grashof (buoyancy) numbers, identifying a mushroom-shaped plume which was observed to detract in length and thickness with increasing Grashof number. He further computed flow separation at high Grashof number and an associated recirculation vortex arising in the wake of the sphere. Furthermore this study showed that local Nusselt number along the sphere surface initially falls, attaining a minimum, and thereafter rises markedly in the vicinity of sphere rear. Sharma and Bhatnagar [30] used the Van Dyke method of matched asymptotic expansions to obtain solutions for creeping heat transfer (viscous-dominated flow) from a spherical body to power-law fluids. Bég et al. [31] examined the free convection magnetohydrodynamic flow from a sphere in porous media using network simulation, showing that temperatures are boosted with magnetic field and heat transfer is enhanced from the lower stagnation point towards the upper stagnation point. Potter and Riley [32] used a perturbation expansion approach to evaluate analytically the eruption of boundary layer into plume arising from free convection boundary layers on a sphere with strong buoyancy effects. Prhashanna and Chhabra [33] obtained numerical solutions for streamline and temperature contours in heat transfer from a heated sphere immersed in quiescent power-law fluids, showing that shear-thinning behavior may elevate heat transfer rates by 300%, whereas shear-thickening depletes heat transfer rates by 30–40% compared with Newtonian fluids. Further interesting investigations of heat transfer from spheres have been presented by Chen and Chen [34] for power-law fluids in porous media, Dhole et al. [35] for forced convection in power-law fluids using the finite volume method and by Bég et al. [36] for combined heat and species diffusion in micropolar fluids with cross-diffusion effects. Prasad et al. [37] have also studied radiative heat flux effects on magneto-convective heat and species diffusion from a sphere in an isotropic permeable medium.

The objective of the present study was to investigate the laminar boundary layer flow and heat transfer of a *Tangent Hyperbolic* non-Newtonian fluid from a sphere. The non-dimensional equations with associated dimensionless boundary conditions constitute a highly nonlinear, coupled two-point boundary value problem. Keller's implicit finite difference "box" scheme is implemented to solve the problem [37]. The effects of the emerging thermophysical parameters, namely *the Weissenberg number (We), power law index (n), Biot number (γ) and Prandtl number (Pr)*, on the velocity, temperature, Skin friction number, and heat transfer rate (local Nusselt number) characteristics are studied. The present problem has to the authors' knowledge not appeared thus far in the scientific literature and is relevant to polymeric manufacturing processes in chemical engineering.

2. Non-Newtonian constitutive Tangent Hyperbolic fluid model

In the present study a subclass of non-Newtonian fluids known as the *Tangent Hyperbolic fluid* is employed owing to its simplicity. The Cauchy stress tensor, in the *Tangent Hyperbolic* non-Newtonian fluid [15] takes the following form:

$$\overline{\tau} = \left[\mu_\infty + (\mu_0 + \mu_\infty)\tanh\left(\Gamma\overline{\dot{\gamma}}\right)^n\right]\overline{\dot{\gamma}} \tag{1}$$

where $\overline{\tau}$ is extra stress tensor, μ_∞ is the infinite shear rate viscosity, μ_0 is the zero shear rate viscosity, Γ is the time

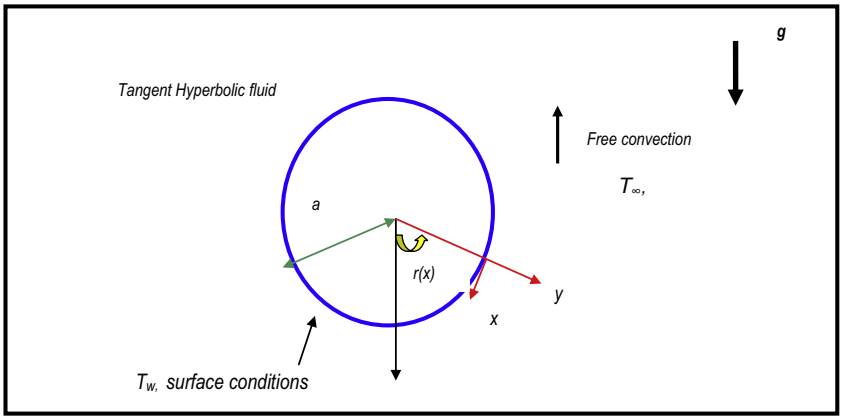

Figure 1 Physical model and coordinate system.

dependent material constant, n is the power law index i.e. flow behavior index and $\bar{\dot{\gamma}}$ is defined as

$$\bar{\dot{\gamma}} = \sqrt{\frac{1}{2}\sum_i\sum_j \bar{\dot{\gamma}}_{ij}\bar{\dot{\gamma}}_{ji}} = \sqrt{\frac{1}{2}\Pi} \tag{2}$$

where $\Pi = \frac{1}{2}tr\left(gradV + (gradV)^T\right)^2$. We consider Eq. (1), for the case when $\mu_\infty = 0$ because it is not possible to discuss the problem for the infinite shear rate viscosity and since we are considering tangent hyperbolic fluid that describes shear thinning effects so $\Gamma\bar{\dot{\gamma}} \ll 1$. Then Eq. (1) takes the form

$$\begin{aligned}\bar{\tau} &= \mu_0\left[\left(\Gamma\bar{\dot{\gamma}}\right)^n\right]\bar{\dot{\gamma}} = \mu_0\left[\left(1+\Gamma\bar{\dot{\gamma}}-1\right)^n\right]\bar{\dot{\gamma}} \\ &= \mu_0\left[1+n\left(\Gamma\bar{\dot{\gamma}}-1\right)\right]\bar{\dot{\gamma}}\end{aligned} \tag{3}$$

The introduction of the appropriate terms into the flow model is considered next. The resulting boundary value problem is found to be well-posed and permits an excellent mechanism for the assessment of rheological characteristics on the flow behavior.

3. Mathematical flow model

Steady, double-diffusive, laminar, incompressible flow of a Tangent Hyperbolic fluid from an sphere, is considered, as illustrated in Fig. 1. The x-coordinate (tangential) is measured along the surface of the sphere from the lowest point and the y-coordinate (radial) is directed perpendicular to the surface, with a denoting the radius of the sphere. $r(x) = a\sin(x/a)$ is the radial distance from the symmetrical axis to the surface of the sphere. The gravitational acceleration $\boldsymbol{g}$, acts downwards. We also assume that the Boussinesq approximation holds i.e. that density variation is only experienced in the buoyancy term in the momentum equation.

Both sphere and the Tangent Hyperbolic fluid are maintained initially at the same temperature. Instantaneously they are raised to a temperature $T_w > T_\infty$, the ambient temperature of the fluid which remains unchanged. In line with the approach of Yih [38] and introducing the boundary layer approximations, the equations for *mass, momentum, and energy*, can be written as follows:

$$\frac{\partial(ru)}{\partial x} + \frac{\partial(rv)}{\partial y} = 0 \tag{4}$$

$$\begin{aligned}u\frac{\partial u}{\partial x} + v\frac{\partial u}{\partial y} &= \nu(1-n)\frac{\partial^2 u}{\partial y^2} + \sqrt{2}\nu n\Gamma\left(\frac{\partial u}{\partial y}\right)\frac{\partial^2 u}{\partial y^2} \\ &\quad + g\beta\sin\left(\frac{x}{a}\right)(T-T_\infty)\end{aligned} \tag{5}$$

$$u\frac{\partial T}{\partial x} + v\frac{\partial T}{\partial y} = \alpha\frac{\partial^2 T}{\partial y^2} \tag{6}$$

where u and v are the velocity components in the x- and y-directions respectively, $\nu = \mu/\rho$ is the kinematic viscosity of the Tangent Hyperbolic fluid, β is the coefficient of thermal expansion, α is the thermal diffusivity, β is the temperature, and ρ is the density of the fluid. The Tangent Hyperbolic fluid model therefore introduces a *mixed* derivative (second order, first degree) into the momentum boundary layer Eq. (5). The

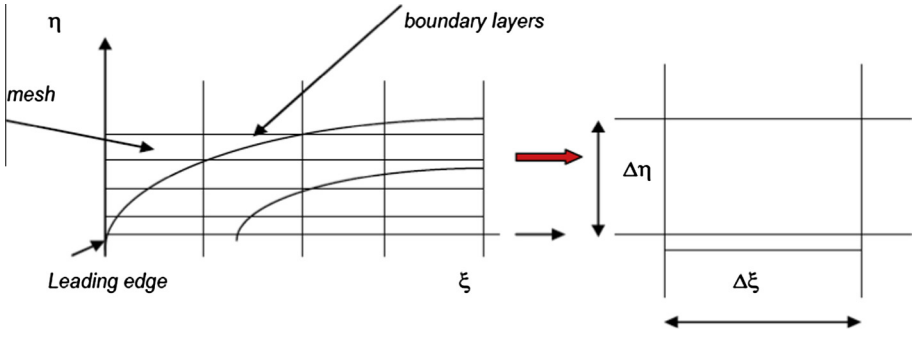

Figure 2 Keller Box computational domain.

Table 1 Values of $f''(\xi,0)$ and $-\theta'(\xi,0)$ for different We, n, and ξ ($Pr = 7.0, \gamma = 0.2$).

We	n	$\xi = 0$		$\xi = \pi/6$		$\xi = \pi/4$	
		$f''(\xi,0)$	$-\theta'(\xi,0)$	$f''(\xi,0)$	$-\theta'(\xi,0)$	$f''(\xi,0)$	$-\theta'(\xi,0)$
0.0	0.3	0	0.1098	0.0573	0.1074	0.0781	0.1053
0.5		0	0.1095	0.0555	0.1071	0.0758	0.1050
1.0		0	0.1093	0.0539	0.1069	0.0736	0.1048
2.0		0	0.1088	0.0508	0.1064	0.0696	0.1044
3.0		0	0.1083	0.0481	0.1060	0.0659	0.1039
4.0		0	0.1079	0.0455	0.1056	0.0624	0.1035
5.0		0	0.1074	0.0432	0.1052	0.0593	0.1032
0.3	0.0	0	0.1020	0.0637	0.0998	0.0896	0.0978
	0.1	0	0.1042	0.0615	0.1020	0.0839	0.1000
	0.2	0	0.1068	0.0590	0.1044	0.0805	0.1024
	0.4	0	0.1129	0.0529	0.1105	0.0723	0.1083
	0.5	0	0.1169	0.0490	0.1143	0.0669	0.1121
	0.6	0	0.1216	0.0440	0.1190	0.0601	0.1166

Table 2 Values of $f''(\xi,0)$ and $-\theta'(\xi,0)$ for different We, n, and ξ ($Pr = 7.0, \gamma = 0.2$).

We	n	$\xi = \pi/3$		$\xi = \pi/2$		$\xi = 2\pi/3$	
		$f''(\xi,0)$	$-\theta'(\xi,0)$	$f''(\xi,0)$	$-\theta'(\xi,0)$	$f''(\xi,0)$	$-\theta'(\xi,0)$
0.0	0.3	0.1057	0.1008	0.1379	0.0898	0.1479	0.0733
0.5		0.1027	0.1006	0.1345	0.0896	0.1449	0.0732
1.0		0.0999	0.1002	0.1313	0.0895	0.1421	0.0732
2.0		0.0946	0.1000	0.1252	0.0892	0.1367	0.0730
3.0		0.0898	0.0996	0.1196	0.0889	0.1317	0.0728
4.0		0.0854	0.0993	0.1144	0.0886	0.1269	0.0726
5.0		0.0813	0.0989	0.1095	0.0883	0.1224	0.0725
0.3	0.0	0.1176	0.0937	0.1535	0.0835	0.1649	0.0683
	0.1	0.1135	0.0958	0.1483	0.0853	0.1593	0.0698
	0.2	0.1090	0.0981	0.1424	0.0874	0.1531	0.0714
	0.4	0.0979	0.1038	0.1282	0.0924	0.1380	0.0755
	0.5	0.0907	0.1074	0.1191	0.0952	0.1285	0.0780
	0.6	0.0817	0.1117	0.1076	0.0995	0.1167	0.0812

Table 3 Values of $f''(\xi,0)$ and $-\theta'(\xi,0)$ for different γ, Pr and ξ ($We = 0.3$, $n = 0.3$).

γ	Pr	$\xi = 0.0$		$\xi = \pi/6$		$\xi = \pi/4$	
		$f''(\xi,0)$	$-\theta'(\xi,0)$	$f''(\xi,0)$	$-\theta'(\xi,0)$	$f''(\xi,0)$	$-\theta'(\xi,0)$
0.2	7	0	0.1096	0.0562	0.1072	0.0767	0.1051
0.3		0	0.3730	0.1150	0.3649	0.1571	0.3577
0.4		0	0.5237	0.1398	0.5122	0.1910	0.5022
0.5		0	0.6185	0.1538	0.6051	0.2101	0.5933
0.7		0	0.7306	0.1691	0.7147	0.2310	0.7008
0.8		0	0.7663	0.1737	0.7497	0.2374	0.7351
1.0		0	0.8169	0.1802	0.7992	0.2462	0.7836
0.2	10	0	0.1185	0.0549	0.1152	0.0750	0.1136
	15	0	0.1330	0.0505	0.1301	0.0689	0.1276
	25	0	0.1534	0.0453	0.1500	0.0618	0.1471
	50	0	0.1851	0.0388	0.1811	0.530	0.1776
	75	0	0.2062	0.0354	0.2018	0.0504	0.1979
	100	0	0.2225	0.0331	0.2177	0.0452	0.2135

Table 4 Values of $f''(\xi,0)$ and $-\theta'(\xi,0)$ for different γ, Pr and ξ ($We = 0.3$, $n = 0.3$, $M = 1.0$).

γ	Pr	$\xi = \pi/3$		$\xi = \pi/2$		$\xi = 2\pi/3$	
		$f''(\xi,0)$	$-\theta'(\xi,0)$	$f''(\xi,0)$	$-\theta'(\xi,0)$	$f''(\xi,0)$	$-\theta'(\xi,0)$
0.2	7	0.1039	0.1007	0.1359	0.0897	0.1461	0.0733
0.3		0.2128	0.3428	0.2790	0.3053	0.3009	0.2495
0.4		0.2589	0.4812	0.3398	0.4287	0.3669	0.3504
0.5		0.2849	0.5684	0.3741	0.5064	0.4043	0.4140
0.7		0.3134	0.6714	0.4117	0.5982	0.4453	0.4891
0.8		0.3220	0.7043	0.4231	0.6275	0.4578	0.5131
1.0		0.3340	0.7508	0.4389	0.6690	0.4751	0.5470
0.2	10	0.1015	0.1089	0.1327	0.0970	0.1428	0.0794
	15	0.0933	0.1223	0.1220	0.1090	0.1315	0.0893
	25	0.0836	0.1410	0.1094	0.1258	0.1181	0.1033
	50	0.0717	0.1702	0.0939	0.1519	0.1015	0.1249
	75	0.0654	0.1897	0.0857	0.1693	0.0926	0.1393
	100	0.0612	0.2046	0.0802	0.1827	0.0867	0.1504

non-Newtonian effects feature in the shear terms only of Eq. (5) and not the convective (acceleration) terms. The third term on the right hand side of Eq. (5) represents the *thermal buoyancy force* and couples the velocity field with the temperature field Eq. (6).

$$\text{At} \quad y = 0, \quad u = 0, \quad v = 0, \quad -k\frac{\partial T}{\partial y} = h_w(T_w - T)$$

$$\text{As} \quad y \to \infty, \quad u \to 0, \quad T \to T_\infty \tag{7}$$

Here T_∞ is the free stream temperature, k is the thermal conductivity, h_w is the convective heat transfer coefficient, and T_w is the convective fluid temperature. The stream function ψ is defined by $ru = \frac{\partial(r\psi)}{\partial y}$ and $rv = -\frac{\partial(r\psi)}{\partial x}$, and therefore, the continuity equation is automatically satisfied. In order to render the governing equations and the boundary conditions in dimensionless form, the following non-dimensional quantities are introduced:

$$\xi = \frac{x}{a}, \quad \eta = \frac{y}{a}Gr^{1/4}, \quad f = \frac{\psi}{v\xi}Gr^{-1/4}, \quad \theta(\xi,\eta) = \frac{T - T_\infty}{T_w - T_\infty}$$
$$Pr = \frac{v}{\alpha}, \quad Gr = \frac{g\beta_1(T_w - T_\infty)a^3}{v^2}, \quad We = \frac{\sqrt{2}v\Gamma x Gr^{3/4}}{a^3} \tag{8}$$

All terms are defined in the nomenclature. In view of the transformation defined in Eq. (8), the boundary layer Eqs. (5)–(7) are reduced to the following coupled, nonlinear, dimensionless partial differential equations for momentum and energy for the regime:

$$(1-n)f''' + (1 + \xi\cot\xi)ff'' - (f')^2 + nWef''f''' + \theta\frac{\sin\xi}{\xi} = \xi\left(f'\frac{\partial f'}{\partial\xi} - f''\frac{\partial f}{\partial\xi}\right) \tag{9}$$

$$\frac{\theta''}{Pr} + (1 + \xi\cot\xi)f\theta' = \xi\left(f'\frac{\partial\theta}{\partial\xi} - \theta'\frac{\partial f}{\partial\xi}\right) \tag{10}$$

The transformed dimensionless boundary conditions are as follows:

$$\text{At} \quad \eta = 0, \quad f = 0, \quad f' = 0, \quad \theta = 1 + \frac{\theta'}{\gamma}$$

$$\text{As} \quad \eta \to \infty, \quad f' \to 0, \quad \theta \to 0 \tag{11}$$

Here primes denote the differentiation with respect to η. The wall thermal boundary condition in (11) corresponds to convective cooling. The skin-friction coefficient (shear stress at the sphere surface) and Nusselt number (heat transfer rate) can be defined using the transformations described above with the following expressions:

$$Gr^{-3/4}C_f = (1-n)\xi f''(\xi,0) + \frac{n}{2}We\xi(f''(\xi,0))^2 \tag{12}$$

$$Gr^{-1/4}Nu = -\theta'(\xi,0) \tag{13}$$

The location, $\xi \sim 0$, corresponds to the vicinity of the *lower stagnation point* on the sphere.

Since $\frac{\sin\xi}{\xi} \to 0/0$ i.e., 1. For this scenario, the model defined by Eqs. (9) and (10) contracts to an *ordinary* differential boundary value problem:

$$(1-n)f''' + ff'' - (f')^2 + nWef''f''' + \theta = 0 \tag{14}$$

$$\frac{1}{Pr}\theta'' + f\theta' = 0 \tag{15}$$

The general model is solved using a powerful and unconditionally stable finite difference technique introduced by Keller [39]. The Keller-box method has a second order accuracy with arbitrary spacing and attractive extrapolation features.

4. Numerical solution with Keller Box implicit method

The Keller-Box implicit difference method is implemented to solve the nonlinear boundary value problem defined by Eqs. (9) and (10) with boundary conditions (11). This technique, despite recent developments in other numerical methods, remains a powerful and very accurate approach for parabolic boundary layer flows. It is unconditionally stable and achieves exceptional accuracy [39]. Recently this method has been deployed in resolving many challenging, multi-physical fluid dynamic problems. These include hydromagnetic Sakiadis flow of non-Newtonian fluids [40], nanofluid transport from a stretching sheet [41], radiative rheological magnetic heat transfer [42], water hammer modeling [43], porous media

convection [44] and magnetized viscoelastic stagnation flows [32]. The Keller-Box discretization is *fully coupled* at each step which reflects the physics of parabolic systems – which are also fully coupled. Discrete calculus associated with the Keller-Box scheme has also been shown to be fundamentally different from all other mimetic (physics capturing) numerical methods, as elaborated by Keller [39]. The Keller Box Scheme comprises four stages as follows:

(1) Decomposition of the Nth order partial differential equation system to N first order equations.
(2) Finite Difference Discretization.
(3) Quasilinearization of Non-Linear Keller Algebraic Equations and finally.
(4) Block-tridiagonal Elimination solution of the Linearized Keller Algebraic Equations

Stage 1: Decomposition of Nth order partial differential equation system to N first order equations

Eqs. (9) and (10) subject to the boundary conditions (11) are first cast as a multiple system of first order differential equations. New dependent variables are introduced:

$$u(x,y) = f', \quad v(x,y) = f'', \quad s(x,y) = \theta, \quad t(x,y) = \theta' \tag{16}$$

These denote the variables for velocity, temperature and concentration respectively. Now Eqs. (9) and (10) are solved as a set of fifth order simultaneous differential equations:

$$f' = u \tag{17}$$

$$u' = v \tag{18}$$

$$\theta' = t \tag{19}$$

$$(1-n)v' + (1+\xi\cot\xi)fv - u^2 + nWevv' + s\frac{\sin\xi}{\xi} = \xi\left(u\frac{\partial u}{\partial\xi} - v\frac{\partial f}{\partial\xi}\right) \tag{20}$$

$$\frac{t'}{Pr} + (1+\xi\cot\xi)ft = \xi\left(u\frac{\partial s}{\partial\xi} - t\frac{\partial f}{\partial\xi}\right) \tag{21}$$

where primes denote differentiation with respect to the variable, η. In terms of the dependent variables, the boundary conditions assume the following form:

$$\text{At} \quad \eta = 0, \quad f = 0, \quad f' = 0, \quad \theta = 1 + \frac{\theta'}{\gamma} \tag{22}$$

$$\text{As} \quad \eta \to \infty, \quad f' \to 0, \quad \theta \to 0 \tag{23}$$

Stage 2: Finite Difference Discretization

A two dimensional computational grid is imposed on the ξ–η plane as depicted in Fig. 2. The stepping process is defined by

$$\eta_0 = 0, \quad \eta_i = \eta_{i-1} + h_j, \quad j = 1, 2, \ldots, J, \quad \eta_J \equiv \eta_\infty \tag{24}$$

$$\xi^0 = 0, \quad \xi^n = \xi^{n-1} + k_n, \quad n = 1, 2, \ldots, N \tag{25}$$

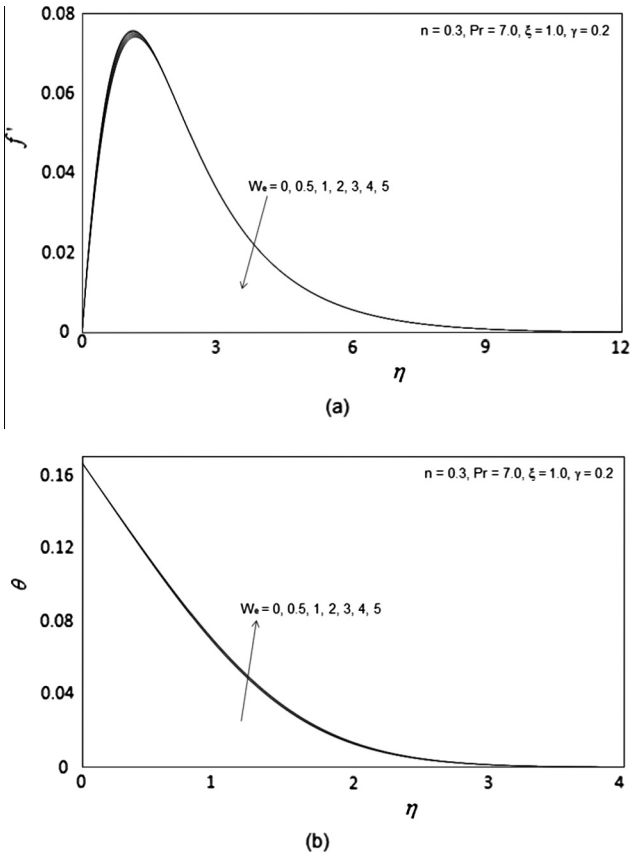

Figure 3 (a) Influence of We on velocity profiles. (b) Influence of We on temperature profiles.

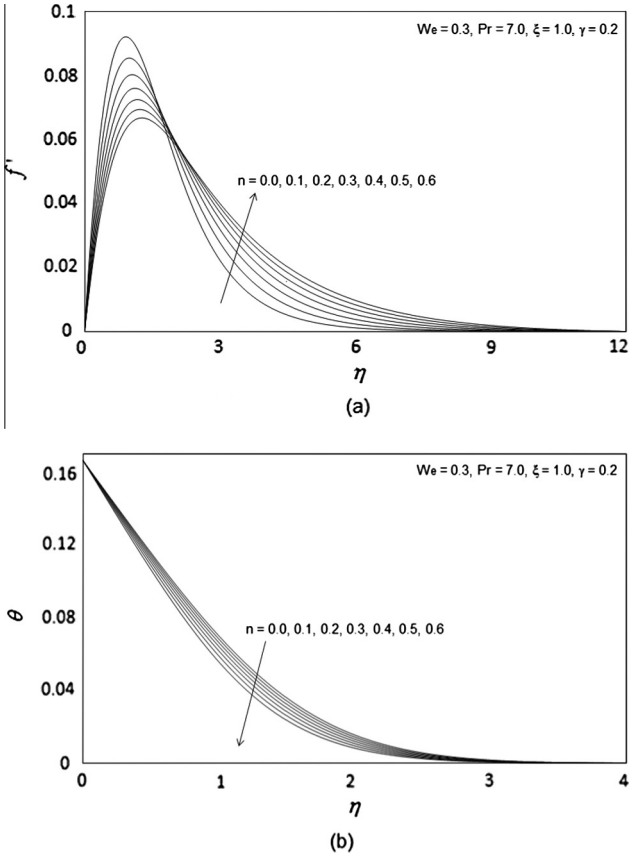

Figure 4 (a) Influence of n on velocity profiles. (b) Influence of n on temperature profiles.

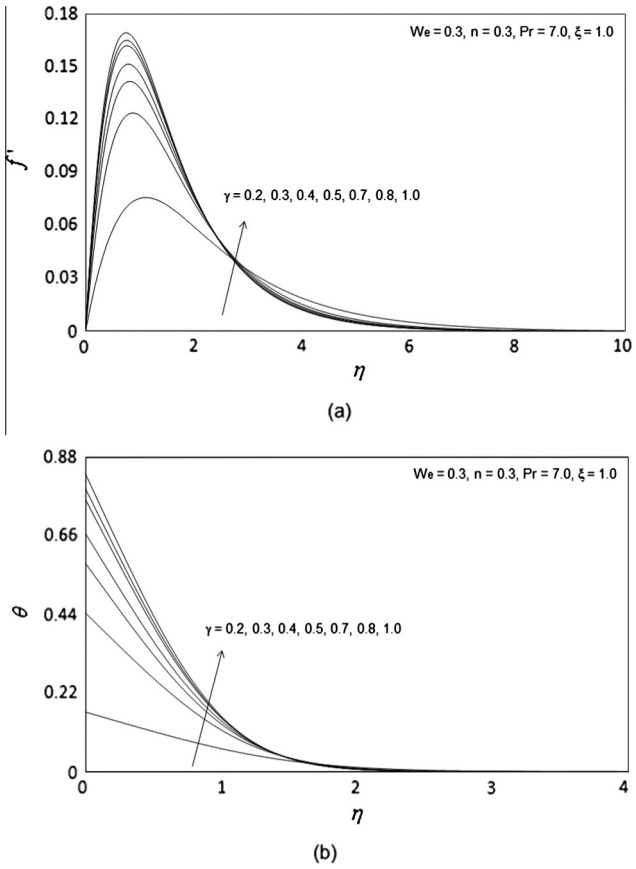

Figure 5 (a) Influence of γ on velocity profiles. (b) Influence of γ on temperature profiles.

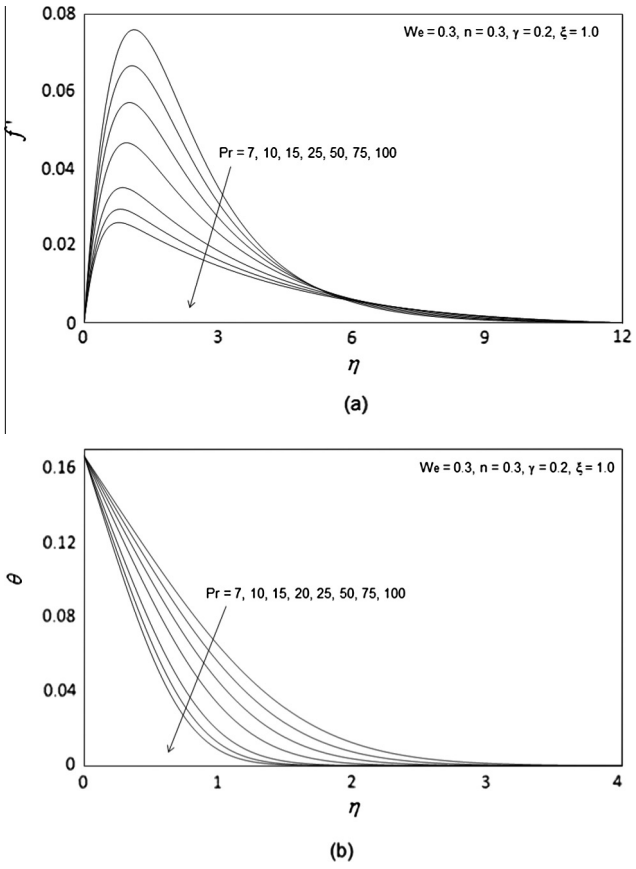

Figure 6 (a) Influence of Pr on velocity profiles. (b) Influence of Pr on temperature profiles.

where k_n is the $\Delta\xi-$ spacing and h_j is the $\Delta\eta-$ spacing.

If g_j^n denotes the value of any variable at (η_j, ξ^n), then the variables and derivatives of Eqs. (17)–(21) at $\left(\eta_{j-1/2}, \xi^{n-1/2}\right)$ are replaced by

$$g_{j-1/2}^{n-1/2} = \frac{1}{4}\left(g_j^n + g_{j-1}^n + g_j^{n-1} + g_{j-1}^{n-1}\right) \tag{26}$$

$$\left(\frac{\partial g}{\partial \eta}\right)_{j-1/2}^{n-1/2} = \frac{1}{2h_j}\left(g_j^n - g_{j-1}^n + g_j^{n-1} - g_{j-1}^{n-1}\right) \tag{27}$$

$$\left(\frac{\partial g}{\partial \xi}\right)_{j-1/2}^{n-1/2} = \frac{1}{2k^n}\left(g_j^n - g_{j-1}^n + g_j^{n-1} - g_{j-1}^{n-1}\right) \tag{28}$$

The finite-difference approximation of Eqs. (17)–(21) for the mid-point $\left(\eta_{j-1/2}, \xi^n\right)$, is

$$h_j^{-1}\left(f_j^n - f_{j-1}^n\right) = u_{j-1/2}^n \tag{29}$$

$$h_j^{-1}\left(u_j^n - u_{j-1}^n\right) = v_{j-1/2}^n \tag{30}$$

$$h_j^{-1}\left(s_j^n - s_{j-1}^n\right) = t_{j-1/2}^n \tag{31}$$

$$\begin{aligned}&(1-n)(v_j - v_{j-1}) + (1+\alpha+\xi\cot\xi)\frac{h_j}{4}(f_j + f_{j-1})(v_j + v_{j-1})\\ &- (1+\alpha)\frac{h_j}{4}(u_j + u_{j-1})^2 + \frac{Bh_j}{2}(s_j + s_{j-1})\\ &+ \frac{nWe}{2}(v_j + v_{j-1})(v_j - v_{j-1}) + \frac{\alpha h_j}{2}v_{j-1}^{n-1}(f_j + f_{j-1})\\ &- \frac{\alpha h_j}{2}f_{j-1}^{n-1}(v_j + v_{j-1}) = [R_1]_{j-/12}^{n-1}\end{aligned} \tag{32}$$

$$\begin{aligned}&\frac{1}{Pr}(t_j - t_{j-1}) + (1+\alpha+\xi\cot\xi)\frac{h_j}{4}(f_j + f_{j-1})(t_j + t_{j-1})\\ &- \frac{\alpha h_j}{4}(u_j + u_{j-1})(s_j + s_{j-1}) + \frac{\alpha h_j}{2}s_{j-1/2}^{n-1}(u_j + u_{j-1})\\ &- \frac{\alpha h_j}{2}u_{j-1/2}^{n-1}(s_j + s_{j-1}) - \frac{\alpha h_j}{2}f_{j-1/2}^{n-1}(t_j + t_{j-1})\\ &+ \frac{\alpha h_j}{2}t_{j-1/2}^{n-1}(f_j + f_{j-1}) = [R_2]_{j-1/2}^{n-1}\end{aligned} \tag{33}$$

where we have used the abbreviations

$$\alpha = \frac{\xi^{n-1/2}}{k_n}, \quad B = \frac{\sin\left(\xi^{n-1/2}\right)}{\xi^{n-1/2}} \tag{34}$$

$$[R_1]_{j-1/2}^{n-1} = -h_j\begin{bmatrix}(1-n)(v')_{j-1/2}^{n-1} + (1-\alpha+\xi\cot\xi)f_{j-1/2}^{n-1}v_{j-1/2}^{n-1}\\ -(1-\alpha)\left(u_{j-1/2}^{n-1}\right)^2 + Bs_{j-1/2}^{n-1} + nWev_{j-1/2}^{n-1}(v')_{j-1/2}^{n-1}\end{bmatrix} \tag{35}$$

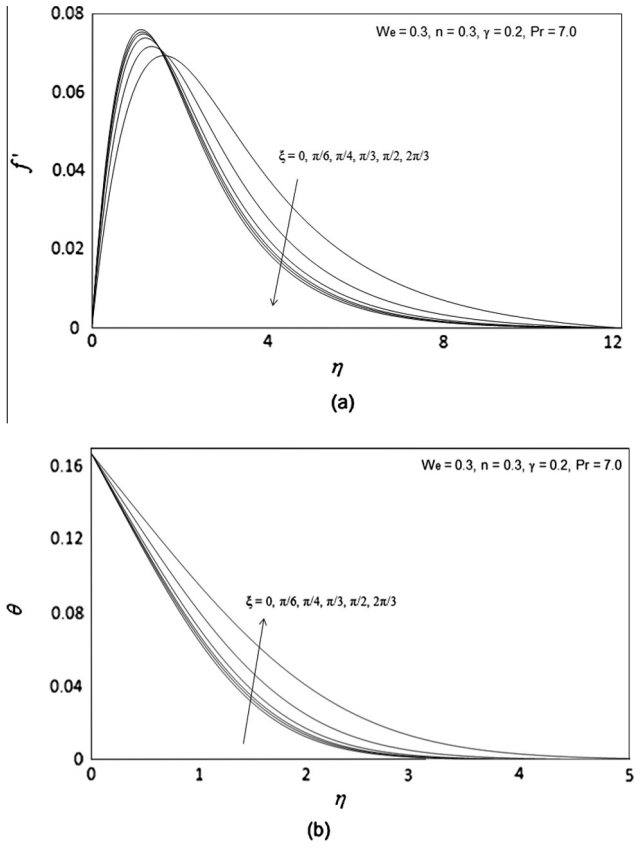

Figure 7 (a) Influence of ξ on velocity profiles. (b) Influence of ξ on temperature profiles.

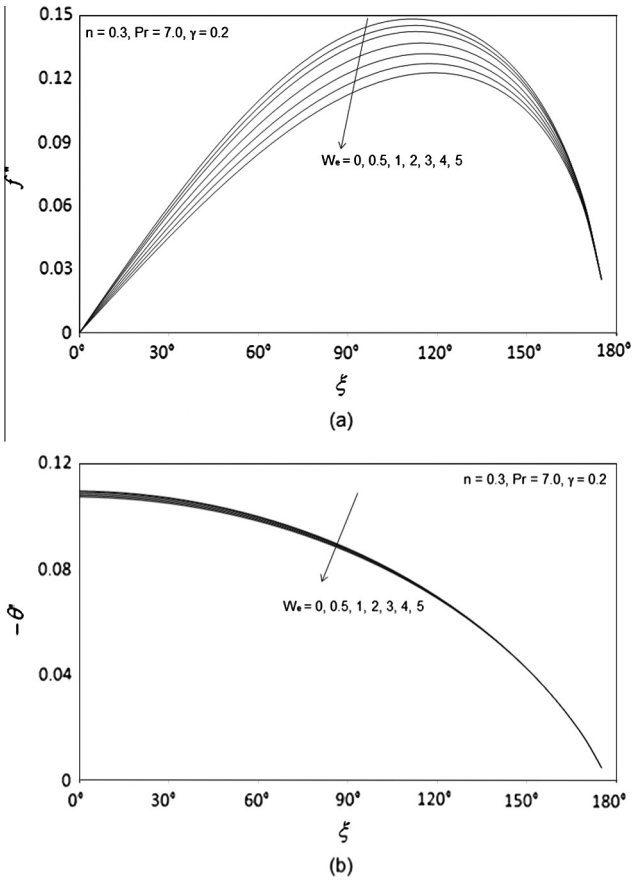

Figure 8 (a) Influence of *We* on Skin friction number. (b) Influence of *We* on local Nusselt number.

$$[R_2]_{j-1/2}^{n-1} = -h_j\left[\frac{1}{Pr}(t')_{j-1/2}^{n-1} + (1-\alpha+\xi\cot\xi)f_{j-1/2}^{n-1}t_{j-1/2}^{n-1} + \alpha u_{j-1/2}^{n-1}s_{j-1/2}^{n-1}\right] \tag{36}$$

The boundary conditions are as follows:

$$f_0^n = u_0^n = 0, \quad s_0^n = 1, \quad u_J^n = 0, \quad v_J^n = 0, \quad s_J^n = 0 \tag{37}$$

Stage 3: Quasilinearization of Non-Linear Keller Algebraic Equations

Assuming $f_j^{n-1}, u_j^{n-1}, v_j^{n-1}, s_j^{n-1}, t_j^{n-1}$ to be known for $0 \leqslant j \leqslant J$, then Eqs. (29)–(33) constitute a system of $5J+5$ equations for the solution of $5J+5$ unknowns $f_j^n, u_j^n, v_j^n, s_j^n, t_j^n$, $j = 0, 1, 2 \ldots, J$. This *non-linear* system of algebraic equations is *linearized* by means of Newton's method as explained in [37,39].

Stage 4: Block-tridiagonal Elimination Solution of Linear Keller Algebraic Equations

The linearized system is solved by the *block-elimination* method, since it possesses a block-tridiagonal structure. The block-tridiagonal structure generated consists of *block matrices*. The complete linearized system is formulated as a *block matrix system*, where each element in the coefficient matrix is a matrix itself, and this system is solved using the efficient Keller-box method. The numerical results are strongly influenced by the number of mesh points in both directions. After some trials in the η-direction (radial coordinate) a larger number of mesh points are selected whereas in the ξ direction (tangential coordinate) significantly less mesh points are utilized. η_{max} has been set at 25 and this defines an adequately large value at which the prescribed boundary conditions are satisfied. ξ_{max} is set at 3.0 for this flow domain. Mesh independence is achieved in the present computations. The numerical algorithm is executed in **MATLAB** on a PC. The method demonstrates excellent stability, convergence and consistency, as elaborated by Keller [39].

5. Numerical results and interpretation

Comprehensive solutions have been obtained and are presented in Tables 1–4 and Figs. 3–9. The numerical problem comprises two independent variables (ξ, η), two dependent fluid dynamic variables (f, θ) and five thermo-physical and body force control parameters, namely, We, n, γ, Pr, ξ. The following default parameter values i.e. $We = 0.3$, $n = 0.3$, $\gamma = 0.2$, $Pr = 0.71$, $\xi = 1.0$ are prescribed (unless otherwise stated). Furthermore the influence of stream-wise (transverse) coordinate on heat transfer characteristics is also investigated.

In Tables 1 and 2, we present the influence of the Weissenberg number (We) and the power law index (n), on the Skin friction and heat transfer rate (Nusselt number), along with a variation in the traverse coordinate (ξ). Increasing We is found to reduce both the Skin friction and local Nusselt numbers. Furthermore an increase in the power law index (n) decreases the skin friction but increases the

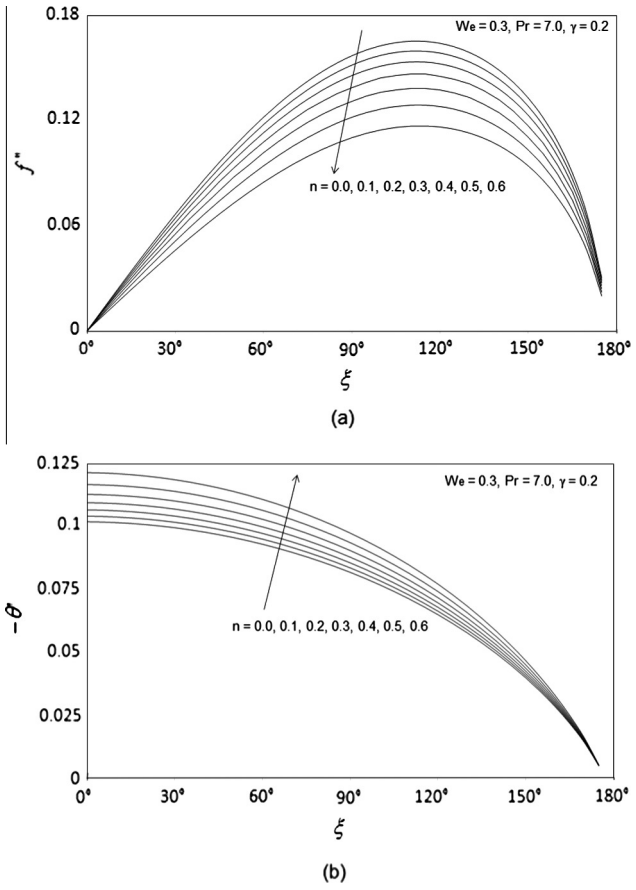

Figure 9 (a) Influence of n on Skin friction number. (b) Influence of n on local Nusselt number.

Nusselt number. Increasing ξ increases the Skin friction whereas the local Nusselt number is decreased.

Tables 3 and 4, document results for the influence of *the Biot number* (γ) and the Prandtl number (Pr) on skin friction and heat transfer rate along with a variation in the traverse coordinate (ξ). Both Skin friction and Nusselt number are increased with increasing γ, whereas increasing ξ, increases the Skin friction but decreases the Nusselt number. These tables also show that with an increase in the Prandtl number, Pr, the skin friction is depressed but the heat transfer rate is elevated.

Fig. 3(a) and (b) depicts the velocity (f') and temperature (θ) distributions with increasing *Weissenberg number, We*. Very little tangible effect is observed in Fig. 3(a), although there is a very slight decrease in velocity with increase in We. Conversely, there is only a very slight increase in temperature magnitudes in Fig. 3(b) with a rise in We. The mathematical model reduces to the *Newtonian viscous flow model* as $We \to 0$ and $n \to 0$. The momentum boundary layer equation in this case contracts to the familiar equation for *Newtonian mixed convection* from a plate, viz. $f''' + (1 + \xi \cot \xi) f f'' - f'^2 + \theta \frac{\sin \xi}{\xi} = \xi \left(f' \frac{\partial f'}{\partial \xi} - f'' \frac{\partial f}{\partial \xi} \right)$. The thermal boundary layer Eq. (10) remains unchanged.

Fig. 4(a) and (b) illustrates the effect of the *power law index*, n, on the velocity (f') and temperature (θ) distributions through the boundary layer regime. Velocity is significantly increased with increasing n. Conversely temperature is consistently reduced with increasing values of n.

Fig. 5(a) and (b) depicts the evolution of velocity (f') and temperature (θ) functions with a variation in Biot number, γ. Dimensionless velocity component (Fig. 5(a)) is considerably enhanced with increasing γ. In Fig. 5(b), an increase in Biot number is seen to considerably enhance temperatures throughout the boundary layer regime. For $\gamma < 1$ i.e. small Biot numbers, the regime is frequently designated as being "thermally simple" and there is a presence of more uniform temperature fields inside the boundary layer and the sphere solid surface. For $\gamma > 1$ thermal fields are anticipated to be non-uniform within the solid body. The Biot number effectively furnishes a mechanism for comparing the conduction resistance within a solid body to the convection resistance external to that body (offered by the surrounding fluid) for heat transfer. We also note that a Biot number in excess of 0.1, as studied in Fig. 5(a) and (b) corresponds to a "thermally thick" substance whereas Biot number less than 0.1 implies a "thermally thin" material. Since γ is inversely proportional to thermal conductivity (k), as γ increases, thermal conductivity will be reduced at the sphere surface and this will lead to a decrease in the rate of heat transfer from the boundary layer to within the sphere, manifesting in a rise in temperature at the sphere surface and in the body of the fluid – the maximum effect will be sustained at the surface, as witnessed in Fig. 5(b). However for a fixed wall convection coefficient and thermal conductivity, Biot number as defined in $\gamma = \frac{x h_w}{k} Gr^{-1/4}$ is also directly inversely proportional to the local Grashof (free convection) number. As local Grashof number increases generally the enhancement in buoyancy causes a deceleration in boundary layer flows [32–34]; however as Biot number increases, the local Grashof number must decrease and this will induce the opposite effect i.e. accelerate the boundary layer flow, as shown in Fig. 5(a).

Fig. 6(a) and (b) depicts the velocity (f') and temperature (θ) distributions with dimensionless radial coordinate, for various transverse (stream wise) coordinate values, ξ. Generally velocity is noticeably lowered with increasing migration from the leading edge i.e. larger ξ values (Fig. 6(a)). The maximum velocity is computed at the *lower stagnation point* ($\xi \sim 0$) for *low values* of radial coordinate (η). The transverse coordinate clearly exerts a significant influence on momentum development. A very strong increase in temperature (θ), as observed in Fig. 6(b), is generated throughout the boundary layer with increasing ξ values. The temperature field *decays monotonically*. Temperature is maximized at the surface of the spherical body (η = 0, for all ξ) and minimized in the free stream (η = 25). Although the behavior at the upper stagnation point ($\xi \sim \pi$) is not computed, the pattern in Fig. 6(b) suggests that temperature will continue to progressively grow here compared with previous locations on the sphere surface (lower values of ξ).

Fig. 7(a) and (b) shows the influence of Weissenberg number, We, on the dimensionless skin friction coefficient $\left((1-n)\xi f''(\xi,0) + \frac{nWe}{2} \xi (f''(\xi,0))^2 \right)$ and heat transfer rate $\theta'(\xi,0)$ at the sphere surface. It is observed that the dimensionless skin friction is decreased with the increase in We i.e. the boundary layer flow is accelerated with decreasing viscosity effects in the non-Newtonian regime. The surface heat transfer rate is also substantially *decreased* with increasing We values.

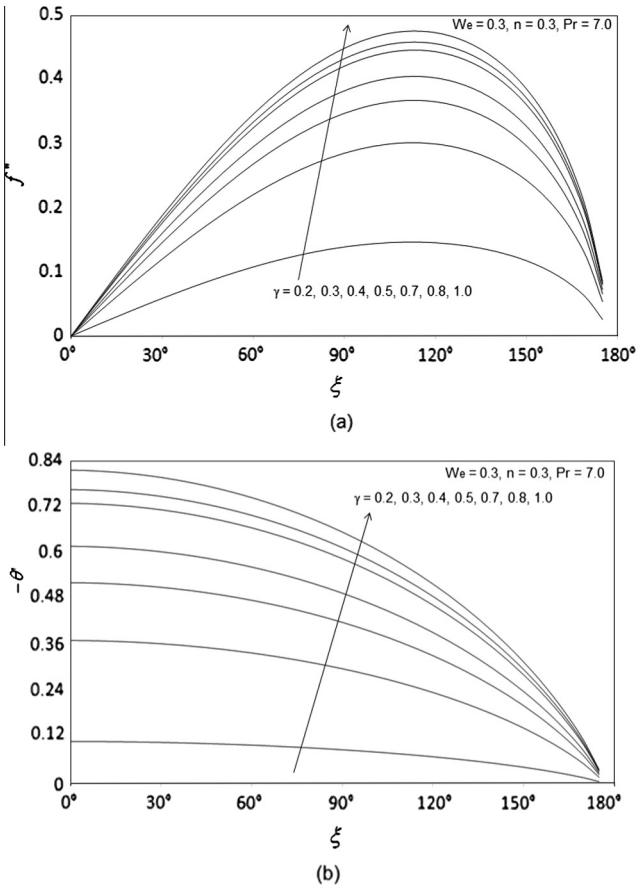

Figure 10 (a) Influence of γ on Skin friction number. (b) Influence of γ on local Nusselt number.

Table 5 Numerical values of $-\theta'(\xi,0)$ for different values of ξ with $We = 0.0$, $n = 0.0$, $\gamma = 0.0$.

ξ	$Pr = 0.7$			$Pr = 7.0$		
	Nazar et al. [45]	Huang and Chen [46]	Present	Nazar et al. [45]	Huang and Chen [46]	Present
0°	0.4576	0.4574	0.4571	0.9595	0.9581	0.9590
10°	0.4565	0.4563	0.4562	0.9572	0.9559	0.9555
20°	0.4533	0.4532	0.4537	0.9506	0.9496	0.9501
30°	0.4480	0.4480	0.4483	0.9397	0.9389	0.9380
40°	0.4405	0.4407	0.4410	0.9239	0.9239	0.9238
50°	0.4308	0.4312	0.4310	0.9045	0.9045	0.9044
60°	0.4189	0.4194	0.4392	0.8801	0.8805	0.8802
70°	0.4046	0.4053	0.4050	0.8510	0.8518	0.8516
80°	0.3879	0.3886	0.3884	0.8168	0.8182	0.8175
90°	0.3684	0.3694	0.3690	0.7774	0.7792	0.7782

Fig. 8(a) and (b) illustrates the influence of the power law index, n, on the dimensionless skin friction coefficient $\left((1-n)\xi f''(\xi,0)+\frac{nWe}{2}\xi(f''(\xi,0))^2\right)$ and heat transfer rate $(\theta'(\xi,0))$. The skin friction (Fig. 8(a)) at the sphere surface is reduced with increasing n, however only for very large values of the transverse coordinate, ξ. However, heat transfer rate (local Nusselt number) is enhanced with increasing n, *again at large values of* ξ, as computed in Fig. 8(b).

Fig. 9(a) and (b) presents the influence of the Biot number, γ, on the dimensionless skin friction coefficient $((1-n)\xi f''(\xi,0)+\frac{nWe}{2}\xi(f''(\xi,0))^2)$ and heat transfer rate $(\theta'(\xi,0))$ at the sphere surface. The skin friction at the sphere surface is found to be greatly increased with rising Biot number, γ. This is principally attributable to the decrease in Grashof (free convection) number which results in an acceleration in the boundary layer flow, as elaborated by Chen and Chen [34]. Heat transfer rate (local Nusselt number) is enhanced with increasing γ, at large values of ξ, as computed in Fig. 9(b).

Figs. 10(a) and 10(b) presents the influence of the Biot number, γ, on the dimensionless skin friction coefficient and heat transfer rate at the sphere surface. The skin friction at the sphere surface is found to be greatly increased with rising Biot number, γ. This is principally attributable to the decrease in Grashof (free convection) number which results in an acceleration in the boundary layer flow, as elaborated by Chen and Chen [46]. Heat transfer rate (local Nusselt number) is enhanced with increasing γ, at large values of x, as computed in Fig. 10(b).

6. Conclusions

Numerical solutions have been presented for the buoyancy-driven flow and heat transfer of Tangent Hyperbolic flow external to an sphere. The Keller-box implicit second order accurate finite difference numerical scheme has been utilized to efficiently solve the transformed, dimensionless velocity and thermal boundary layer equations, subject to realistic boundary conditions. Excellent correlation with previous studies has been demonstrated testifying to the validity of the present code as shown in Table 5. The computations have shown that:

1. Increasing Weissenberg number, *We*, decreases velocity, skin friction (surface shear stress) and heat transfer rate, whereas it increases temperature in the boundary layer.
2. Increasing power law index, n, increases velocity and Nusselt number for all values of radial coordinate i.e., throughout the boundary layer regime whereas it decreases temperature and skin friction.
3. Increasing Biot number, γ, increases velocity, temperature, skin friction (surface shear stress) and heat transfer rate.
4. Increasing transverse coordinate (ξ) generally decelerates the flow near the sphere surface and reduces momentum boundary layer thickness whereas it enhances temperature and therefore increases thermal boundary layer thickness in Tangent Hyperbolic non-Newtonian fluids.

Generally very stable and accurate solutions are obtained with the present finite difference code. The numerical code is able to solve nonlinear boundary layer equations very efficiently and therefore shows excellent promise in simulating transport phenomena in other non-Newtonian fluids.

References

[1] V. Ramachandra Prasad, A. Subba Rao, N. Bhaskar Reddy, B. Vasu, O. Anwar Bég, Modelling laminar transport phenomena in a Casson rheological fluid from a horizontal circular cylinder with partial slip, Proc. Inst. Mech. Eng., E: J Process Mech. Eng. 227 (4) (2013) 309–326.

[2] M. Norouzi, M. Davoodi, O. Anwar Bég, A.A. Joneidi, Analysis of the effect of normal stress differences on heat transfer in creeping viscoelastic Dean flow, Int. J. Therm. Sci. 69 (2013) 61–69.
[3] M.J. Uddin, N.H.M. Yusoff, O. Anwar Bég, A.I. Ismail, Lie group analysis and numerical solutions for non-Newtonian nanofluid flow in a porous medium with internal heat generation, Phys. Scr. 87 (2) (2013) (14pp).
[4] M.M. Rashidi, M. Keimanesh, O. Anwar Bég, T.K. Hung, Magneto-hydrodynamic biorheological transport phenomena in a porous medium: a simulation of magnetic blood flow control, Int. J. Numer. Meth. Biomed. Eng. 27 (6) (2011) 805–821.
[5] D. Tripathi, S.K. Pandey, O. Anwar Bég, Mathematical modelling of heat transfer effects on swallowing dynamics of viscoelastic food bolus through the human oesophagus, Int. J. Therm. Sci. 70 (2013) 41–53.
[6] A. Ishak, Similarity solutions for flow and heat transfer over a permeable surface with convective boundary condition, Appl. Math. Comput. 217 (2) (2010) 837–842.
[7] A. Aziz, A similarity solution for laminar thermal boundary layer over a flat plate with a convective surface boundary condition, Commun. Nonlinear Sci. Numer. Simul. 14 (4) (2009) 1064–1068.
[8] A. Aziz, Hydrodynamic and thermal slip flow boundary layers over a flat plate with constant heat flux boundary condition, Commun. Nonlinear Sci. Numer. Simul. 15 (3) (2010) 573–580.
[9] O.D. Makinde, P.O. Olanrewaju, Buoyancy effects on thermal boundary layer over a vertical plate with a convective surface boundary condition, Trans. ASME J. Fluids Eng. 132 (4) (2010) 044502 (4pp).
[10] O.D. Makinde, A. Aziz, MHD mixed convection from a vertical plate embedded in a porous medium with a convective boundary condition, Int. J. Therm. Sci. 49 (9) (2010) 1813–1820.
[11] D. Gupta, L. Kumar, O. Anwar Bég, B. Singh, Finite element simulation of mixed convection flow of micropolar fluid over a shrinking sheet with thermal radiation, Proc. IMechE E: J. Process Mech. Eng. 228 (1) (2013) 61–72.
[12] O.D. Makinde, K. Zimba, O. Anwar Bég, Numerical study of chemically-reacting hydromagnetic boundary layer flow with Soret/Dufour effects and a convective surface boundary condition, Int. J. Therm. Environ. Eng. 4 (1) (2012) 89–98.
[13] O. Anwar Bég, M.J. Uddin, M.M. Rashidi, N. Kavyani, Double-diffusive radiative magnetic mixed convective slip flow with Biot number and Richardson number effects, J. Eng. Thermophys. 23 (2) (2014) 79–97.
[14] S.V. Subhashini, N. Samuel, I. Pop, Double-diffusive convection from a permeable vertical surface under convective boundary condition, Int. Commun. Heat Mass Transfer 38 (9) (2011) 1183–1188.
[15] I. Pop, D.B. Ingham, Convective Heat Transfer: Mathematical and Computational Modelling of Viscous Fluids and Porous Media, Pergamon, Amsterdam, NewYork, 2001.
[16] S. Nadeem, S. Akram, Peristaltic transport of a hyperbolic tangent fluid model in an asymmetric channel, ZNA 64a (2009) 559–567.
[17] S. Nadeem, S. Akram, Magnetohydrodynamic peristaltic flow of a hyperbolic tangent fluid in a vertical asymmetric channel with heat transfer, Acta Mech. Sin. 27 (2) (2011) 237–250.
[18] Akram Safia, Nadeem Sohail, Simulation of heat and mass transfer on peristaltic flow of hyperbolic tangent fluid in an asymmetric channel, Int. J. Numer. Methods Fluids 70 (12) (2012) 1475–1493.
[19] N.S. Akbar, S. Nadeem, R.U. Haq, Z.H. Khan, Numerical solution of Magnetohydrodynamic boundary layer flow of Tangent Hyperbolic fluid towards a stretching sheet, Indian J. Phys. 87 (11) (2013) 1121–1124.
[20] Noreen Sher Akbar, Peristaltic flow of Tangent Hyperbolic fluid with convective boundary condition, Eur. Phys. J. Plus 129 (2014) 214.
[21] S. Nadeem, Sadaf Ashiq, Noreen Sher Akbar, Changhoon Lee, Peristaltic flow of hyperbolic tangent fluid in a diverging tube with heat and mass transfer, J. Energy Eng. 139 (2) (2013) 124–135.
[22] Noreen Sher Akbar, T. Hayat, S. Nadeem, S. Obaidat, Peristaltic flow of a Tangent Hyperbolic fluid in an inclined asymmetric channel with slip and heat transfer, Prog. Comput. Fluid Dyn. 12 (5) (2012) 363–374.
[23] Noreen Sher Akbar, S. Nadeem, T. Hayat, Awatif A. Hendi, Effects of heat and mass transfer on the peristaltic flow of hyperbolic tangent fluid in an annulus, Int. J. Heat Mass Transfer 54 (2011) 4360–4369.
[24] W.S. Amato, T. Chi, Free convection heat transfer from isothermal spheres in water, Int. J. Heat Mass Transfer 15 (1972) 327–339.
[25] K.S. Liew, M. Adelman, Laminar natural heat transfer from an isothermal sphere to non-Newtonian fluids, Can. J. Chem. Eng. 53 (5) (1975) 494–499.
[26] W.S. Amato, T. Chi, Free convection heat transfer from isothermal spheres in polymer solutions, Int. J. Heat Mass Transfer 19 (11) (1976) 1257–1266.
[27] S.W. Churchill, Comprehensive, theoretically based, correlating equations for free convection from isothermal spheres, Chem. Eng. Commun. 24 (4–6) (1983) 339–352.
[28] F-S Lien, C-K Chen, Mixed convection of micropolar fluid about a sphere with blowing and suction, Int. J. Eng. Sci. 25 (7) (1987) 775–784.
[29] H. Jia, G. Gogos, Laminar natural convection transfer from isothermal spheres, Int. J. Heat Mass Transfer 39 (8) (1996) 1603–1615.
[30] O.P. Sharma, R.K. Bhatnagar, Low Reynolds number heat transfer from a sphere in a laminar flow of non-Newtonian fluids, ZAMM – Z. Angew. Math. Mech. 55 (5) (1975) 235–242.
[31] O. Anwar Bég, J. Zueco, R. Bhargava, H.S. Takhar, Magnetohydrodynamic convection flow from a sphere to a non-Darcian porous medium with heat generation or absorption effects: network simulation, Int. J. Therm. Sci. 48 (5) (2009) 913–921.
[32] J.N. Potter, N. Riley, Free convection from a heated sphere at large Grashof number, J. Fluid Mech. 100 (4) (1980) 769–783.
[33] A. Prhashanna, R.P. Chhabra, Free convection in power-law fluids from a heated sphere, Chem. Eng. Sci. 65 (23) (2010) 6190–6205.
[34] H-T. Chen, C-K. Chen, Natural convection of a non-Newtonian fluid about a horizontal cylinder and a sphere in a porous medium, Int. Commun. Heat Mass Transfer 15 (5) (1988) 605–614.
[35] S.D. Dhole, R.P. Chhabra, V. Eswaran, Forced convection heat transfer from a sphere to non-Newtonian power law fluids, AIChemE J. 52 (11) (2006) 3658–3667.
[36] O. Anwar Bég, V.R. Prasad, B. Vasu, N. Bhaskar Reddy, Q. Li, R. Bhargava, Free convection heat and mass transfer from an isothermal sphere to a micropolar regime with Soret/Dufour effects, Int. J. Heat Mass Transfer 54 (1–3) (2011) 9–18.
[37] V.R. Prasad, B. Vasu, O. Anwar Bég, D.R. Parshad, Thermal radiation effects on magnetohydrodynamic free convection heat and mass transfer from a sphere in a variable porosity regime, Commun. Nonlinear Sci. Numer. Simul. 17 (2) (2012) 654–671.
[38] K.A. Yih, Viscous and Joule Heating effects on non-Darcy MHD natural convection flow over a permeable sphere in porous media with internal heat generation, Int. Commun. Heat Mass Transfer 27 (4) (2000) 591–600.
[39] H.B. Keller, Numerical methods in boundary-layer theory, Ann. Rev. Fluid Mech. 10 (1978) 417–433.

[40] M. Subhas Abel, P.S. Datti, N. Mahesha, Flow and heat transfer in a power-law fluid over a stretching sheet with variable thermal conductivity and non-uniform heat source, Int. J. Heat Mass Transfer 52 (11–12) (2009) 2902–2913.
[41] K. Vajravelu, K.V. Prasad, J. Lee, C. Lee, I. Pop, Robert A. Van Gorder, Convective heat transfer in the flow of viscous Ag–water and Cu–water nanofluids over a stretching surface, Int. J. Therm. Sci. 50 (5) (2011) 843–851.
[42] C.-H. Chen, Magneto-hydrodynamic mixed convection of a power-law fluid past a stretching surface in the presence of thermal radiation and internal heat generation/absorption, Int. J. Non-Linear Mech. 44 (6) (2009) 596–603.
[43] Y.L. Zhang, K. Vairavamoorthy, Analysis of transient flow in pipelines with fluid–structure interaction using method of lines, Int. J. Numer. Methods Eng. 63 (10) (2005) 1446–1460.
[44] Orhan Aydın, Ahmet Kaya, Non-Darcian forced convection flow of viscous dissipating fluid over a flat plate embedded in a porous medium, Transp. Porous Media 73 (73) (2008) 173–186.
[45] R. Nazar, N. Amin, T. Grosan, I. Pop, Free convection boundary layer on an isothermal sphere in a micropolar fluid, Int. Comm. Heat Mass Transfer 29 (2002) 377–386.
[46] M.J. Huang, C.K. Chen, Laminar free convection from a sphere with blowing and suction, J. Heat Transfer 109 (1987) 529–532.